This article has been accepted for publication in a future issue of this journal, but has not been fully edited. Content may change prior to final publication. Citation information: DOI 10.1109/TCOMM.2019.2936354, IEEE Transactions on Communications

Joint Location and Beamforming Design for Cooperative UAVs with Limited Storage Capacity

Phuc Dinh, Tri Minh Nguyen, *Student Member, IEEE* Sanaa Sharafeddine, *Senior Member, IEEE*, and Chadi Assi, *Senior Member, IEEE*

***Abstract*—In this paper, we investigate downlink transmissions in a wireless communication system enabled by a swarm of unmanned aerial vehicles (UAVs) which are spatially dispatched to cooperatively deliver requested contents to ground users. First, we propose a communication scheme that exploits the flexible deployment of UAVs as well as their cooperative transmissions to improve in-network user admission. Unlike previous literature, a practical operational constraint of limited storage capacity for UAVs is considered. Then, from the knowledge that cooperation among UAVs depends on the availability of the contents in their limited storage space, we propose a novel joint optimization problem to determine the content placement, location planning, user admission decision and transmit beamforming to maximize the number of users experiencing a minimum required rate, so-called admitted users. Since the formulated problem is a mixed-integer non-linear program which is generally non-deterministic polynomial-time hard, we proposed a framework that is developed on the basis of difference-of-convex (DC) programming to transform the original problem into a series of approximate convex problems which can be iteratively solved until convergence. Our extensive simulation results reveal that the proposed scheme outperforms other schemes that have been introduced in previous work and reflect a notable trend that deploying more cooperative UAVs with fewer resources (power and storage capacity) is more efficient than deploying fewer UAVs with more resources. In particular, in one of our collected results, the total communication power can be reduced by roughly 40 dB when doubling the number of cooperative UAVs.**

***Index Terms*—Unmanned aerial vehicle, beamforming, optimization, difference-of-convex programming.**

I. Introduction

Future wireless communication technologies are under development to adapt to different application scenarios of 5G and beyond (5G/B5G). Specifically, Enhanced Mobile Broadband (eMBB), Massive Machine-Type Communication (mMTC) and Ultra-Reliable Low-Latency Communication (URLLC), also called mission-critical communications, are widely considered the key services in 5G [1]. In other words, 5G networks are expected to accommodate a huge number of mobile devices with heterogeneous and stringent requirements in terms of data rate, latency, and reliability. To meet the heightened expectations for 5G, numerous wireless technologies have been developed including mmWave communications [2], massive MIMO [3], or ultra-densification [4]. However, capacity-enhancing solutions such as installing more cell sites (ultra-densification) or using additional spectrum (mmWave) are costly and may sometimes lead to underutilization of resources due to the time-varying network traffic. Thus, an alternative is to integrate a highly flexible communication platform that can be swiftly deployed to adapt to the dynamic traffic demand, yet ensure adequate quality of service (QoS).

Recently, the advent of wireless communication systems enabled by unmanned aerial vehicles (UAVs) has attracted significant attention. Compared to the conventional cellular network infrastructure such as ground base stations (GBSs), UAVs are highly mobile, much cheaper and faster to deploy, and able to establish favorable line-of-sight (LoS) communication channels due to their high-altitude deployment for more reliable transmissions [5], [6]. Due to these desirable attributes, UAVs can offer a wide range of applications including coverage expansion [7], data collection [8], computation offloading [9], and mobile relaying [10].

Despite their enormous potential, UAVs reveal some technical limitations hindering their operations in wireless networks such as the SWaP (size, weight, and power) constraints [11]. In other worlds, UAVs can only operate with a low power budget and carry a limited payload of storage, computing, and communication devices. Another major challenge is to manage the severe interference induced by the LoS channels in systems of multiple UAVs [12]. To address these challenges, a proper deployment for UAVs needs to be simultaneously considered with effective communication techniques.

With the recent advances of distributed antenna systems (DAS), multicast beamforming [13] has leveraged the cooperative communications over multiple transmission/reception points and has been realized to be an effective interference mitigation technique and been incorporated in LTE Advanced Releases. While interference management techniques such as power allocation depend only on the handling of signal amplitude, beamforming exploits both amplitudes and phases of the transmitter-receiver channels for proper beamforming design to improve spatial multiplexing gain. In the context of UAV communications, the UAVs can operate as a virtual distributed antenna array whose elements (UAVs) can be swiftly relocated to offer an additional design degree to the original beamforming optimization problem and further enhance macrodiversity gain of DAS. For instance, UAVs can fly closer to target users to reduce the impact of path loss and inter-UAV interference. As a result, joint optimization of beamforming design (beamformers) and location planning for cooperative UAVs, subject to their operational constraints in

P. Dinh and C. Assi are with Concordia University, Montréal, Canada (emails: {p_dinh@encs, assi@ciise}.concordia.ca).

T. M. Nguyen was with e École de Technologie Supérieure (ÉTS), Montréal, Canada (e-mail: minh-tri.nguyen.1@ens.etsmtl.ca).

S. Sharafeddine is with Lebanese American University, Beirut, Lebanon (e-mail: sanaa.sharafeddine@lau.edu.lb)

This article has been accepted for publication in a future issue of this journal, but has not been fully edited. Content may change prior to final publication. Citation information: DOI 10.1109/TCOMM.2019.2936354, IEEE Transactions on Communications

terms of limited power and storage capacity is an appealing, yet challenging problem to address.

A. Related work

Recently, extensive efforts have been dedicated to the study of UAVs' utility in wireless communication systems. In [14] and [15] the authors studied the optimal trajectory of UAVs for computational offloading and data collection, respectively. Besides trajectory design, several works have studied the optimal placement of UAVs for different use cases. Typically, the authors in [16] proposed a low-complexity algorithm for 3-D UAV placement for maximum coverage. Similarly, the positioning problem of UAVs is studied in [17], where a neural network based technique is used to minimize the delay in heterogeneous wireless networks, while the authors in [18] considered the optimal placement of relaying UAVs for maximum communication reliability. The work [19] drew a comparison between the performance of UAVs acting as aerial base stations and traditional terrestrial base stations in terms of average sum rate and transmit power.

One of the major obstacles to exploit the full potential of UAVs lies in their limited flight time. Unlike fixed terrestrial communication infrastructure such as GBSs, the performance of UAV systems is fundamentally limited by the on-board energy [5]. Inspired by this, several works focus on the aspect of energy-efficiency and service time for UAVs. Typically, the authors in [20] studied the communication between a UAV and a ground terminal by optimizing the UAV's trajectory to maximize the energy efficiency as a function of throughput and energy consumption. In [21], a UAV's trajectory is designed to minimize its mission completion time while still ensuring all the ground nodes can recover the disseminated file. However, in these works, the communication systems include only one UAV. In terms of security, [22] performed an analysis for cache-enabled UAVs to assist secure transmission in hyper-dense networks.

Besides UAV-related literature, it is worth noting that interference management with limited storage capacity at the transmitters has been an well-established research topic for networks of fixed infrastructure. Typically, the authors in [23] leveraged tools from stochastic geometry and difference-of-convex (DC) programming to maximize successful transmission probability. However, [23] utilized the multiple antennas at the receivers as a diversity technique without considering multiple cooperative transmissions by exploiting duplicate files at the transmitters. In addition, the swift and cost-effective deployment of UAVs shows more promises for sudden variations for network demand traffic since installing additional infrastructures, such as cache helpers as in [23] or GBSs, is often slow or even economically infeasible.

B. Motivations and contributions

Although there is a fair amount of research on UAV-enabled wireless communication system, most considered single-UAV systems [14]–[16], [18], [20], [21], [24]–[26]. Multi-UAV scenarios are considered in [27] and [28]. However, these works simplify interference management by considering power allocation or using orthogonal resource blocks, which do not fully exploit in-network spatial multiplexing gain. Most recently, Liu *et al* have considered zero-forcing beamforming (ZFBF) for an uplink multi-UAV setup by utilizing multiple receptions at UAVs to improve the minimum throughput [29]. In this paper, we instead focus on multicast beamforming for downlink transmissions, where joint (cooperative) transmissions are influenced not only by location planning but also by strategic content placement for the UAVs. The advantages of our proposed UAV-enabled cooperative communication can be listed as follows.

- **High scalability**: the number of UAVs (antenna elements) can be adjusted on-demand and is not limited by space constraint as in centralized antenna systems. Thus, UAVs can be flexibly added (removed) to (from) the system based on the time-variant network traffic to meet users' QoS requirements or to avoid resource underutilization.
- **Enhanced reliability**: by deploying multiple cooperative UAVs, we alleviate the cost when one node (UAV) is down by reconstructing network topology.
- **Higher energy efficiency**: by replacing a high-power centralized antenna by a group of low-power cooperative UAVs, we reduce the path loss and increase the presence of LoS channels. Hence, each UAV consumes less energy and achieves longer flight time.

In this work, we consider the communication system from a content-centric viewpoint, where the central entities are the "named contents". This viewpoint is especially relevant to the context of 5G and B5G networks with a huge number of subscribers, where the system is no longer a host-centric network but mostly a distribution network [30]. Our contributions in this work can be summarized as follows. [1].

- We propose a network architecture that incorporates multiple cooperative UAVs to serve ground users. In our system, we employ multicast beamforming as the interference management scheme. The UAVs serve the ground users requesting different contents via spatial multiplexing and joint transmissions to achieve their required QoS in terms of transmission rates. The users that experience the (minimum) required QoS are referred to as "admitted users".
- Since the cooperation among UAVs depends on the availability of the contents on each UAV and the location planning, we formulate the joint problem of determining content placement, location planning, admission strategy, and beamforming design to maximize the number of admitted users.
- Our formulation is a mixed-integer non-convex optimization problem which is very difficult to solve in polynomial time. Thus, we propose a framework based on the concept of difference-of-convex (DC) programming to approximate it into a series of convex problems and successively solve them until the results converge.
- We perform extensive numerical results to show that our scheme outperforms previous communication schemes

[1]Part of this work has been presented at the IEEE Wireless Communications and Networking Conference 2019 [31]

This article has been accepted for publication in a future issue of this journal, but has not been fully edited. Content may change prior to final publication. Citation information: DOI 10.1109/TCOMM.2019.2936354, IEEE Transactions on Communications

proposed in the literature and offer some insights by varying some of the system parameters. A notable trend in our results is that increasing the number UAVs remarkably reduce the power consumption per UAVs for the same user admission. This finding offers a possible solution to save power consumption and improve the UAVs' lifetime, which is a major concern in UAV communications.

The rest of the paper is organized as follows. Section II introduces the system model. The problem formulation is presented in III. Section IV proposes the solution approach. Section V presents the development of our low-complexity algorithm. Section VI presents and discusses our numerical results. Finally, conclusions are drawn in Section VII.

Notation: $\mathbf{x}^\intercal$, $\mathbf{x}^\dagger$, $\|\mathbf{x}\|$, $\|\mathbf{x}\|_F$, $\|\mathbf{x}\|_\infty$ are the transpose, Hermitian transpose, 2-norm, Frobenius norm, and infinity norm of vector $\mathbf{x}$, respectively. $\mathbf{x} \circ \mathbf{y}$ is the Hadamard product between vectors $\mathbf{x}$ and $\mathbf{y}$. Bdiag($\mathbf{A}_1$,....,$\mathbf{A}_n$) represents the block diagonal matrix that connects matrices $\mathbf{A}_1$,....,$\mathbf{A}_n$.$|\, x \,|$, x^* and Re(x) are the modulus, conjugate, and real part of complex number x, respectively.

II. System Model

A. Spatial model

We consider a wireless communication system which employs multiple single-antenna UAVs, each integrated with a storage device of limited size and playing the role of aerial base stations to provide delay-tolerant wireless services to the ground users as in Fig. 1. Let us denote $\mathscr{U} = \{0,...,U\}$ as the set of UAVs , $\mathscr{N} = \{1,...,N\}$ as the set of users within a given geographical region, and $\mathscr{K} = \{1,...,K\}$ as the set of contents to be requested, on which we will elaborate further in section II-B. We divide set $\mathscr{N}$ into multiple subsets $\mathscr{N}_k, \forall k \in \mathscr{K}$, where $\mathscr{N}_k$ indicates the group of users requesting the k-th content belonging to set $\mathscr{K}$, which we will call group k from now on. To serve ground users by the UAVs, we apply "*fly-then-hover-and-transmit*" operation as in [32], where rotary-wing UAVs are a good option for deployment. In other words, based on users' locations and content request, the UAVs fly to designated locations and hover there to transmit the requested contents in a cooperative manner. Multiple UAVs can perform beamforming and joint transmission based on the availability of the contents in their storage devices to improve the quality of received signals at the user ends. We consider the relative positions of the users and UAVs to be quasi-static within the period of service. The locations of UAVs can be dynamically adjusted at the next period of service when users' locations change or a new swarm of UAVs can be deployed while the first swarm returns to some docking stations to recharge. For simplicity, each UAV is deployed at a fixed altitude H and denote the coordinate of the i-th UAV as $p_i = \{x_i, y_i, H\}, \forall i \in \mathscr{U}$. For notational convenience, let $\mathbf{p} = \{p_i, \forall i \in \mathscr{U}\}$ be the location vector of all UAVs. Then, let $\{x_{jk}, y_{jk}, 0\}, \forall k \in \mathscr{K}$ denote the position of the j-th user of group k. As a result, the distance between the i-th UAV and the j-th user of group k is $d_{ijk} = \sqrt{(x_{jk}-x_i)^2 + (y_{jk}-y_i)^2 + H^2}$.

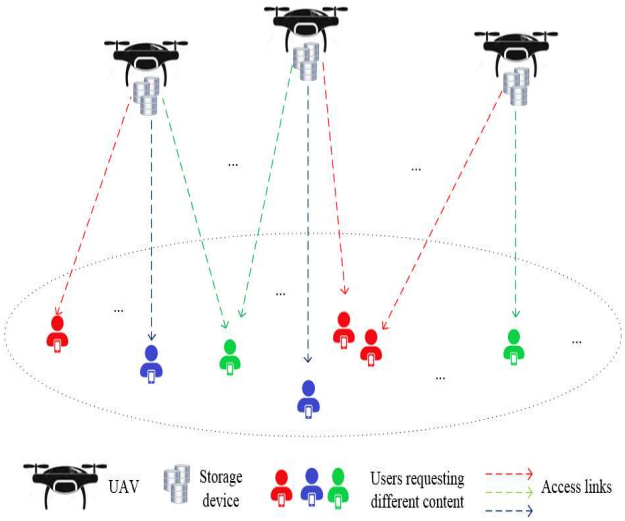

Fig. 1. Cooperative UAVs serving users.

B. Content request distribution model

The $\mathscr{K}$ represents the library of K contents requested by ground users. K is a finite positive integer and the content library follow a popularity order where content k is the k-th most requested one. The random variable k that follows a Zipf distribution for which the probability mass function is given by

$$f(k) = \frac{k^{-\alpha}}{\sum_{i=1}^{K} i^{-\alpha}} \tag{1}$$

where $0 < \alpha < 1$ is the shape parameter that characterizes the Zipf distribution and is considered a priori. The larger α is, the more likely the most popular contents are requested. In other words, α represents the level of concentration of the request distribution around the most popular content. The function $f(k)$ is interpreted as the likelihood that content k is requested. For simplicity, the size of each content is assumed to be 1 and the storage capacity at each UAV is characterized as the maximum number of contents the UAVs can store. However, the concept of our problem can be easily extended to inhomogeneous sizes of contents. We further assume that the content request distribution does not change while the UAVs are serving users. This is a valid assumption regarded by most previous literature.

C. Channel model

In this work, we consider free-space path-loss (FSPL) model with Rician small-scale fading following the authors in [33] and [26].[2]

Let us denote h_{ijk} as the AtG channel from the ith UAV to the jth user in the group k. Specifically, h_{ijk} is a composition

[2]When the UAV's altitude is comparable to the cell radius as in [26], the probability of non-line-of-sight occurrence is negligible. This can be easily verified using the expression of LoS probability included in some relevant channel modeling literature such as [6].

This article has been accepted for publication in a future issue of this journal, but has not been fully edited. Content may change prior to final publication. Citation information: DOI 10.1109/TCOMM.2019.2936354, IEEE Transactions on Communications

of the small-scale fading coefficient $\tilde{h}_{ijk}$, $\mathbf{E}(|\tilde{h}_{ijk}|^2 = 1)$ and the path-loss coefficient θ_{ijk} which is given by

$$h_{ijk}(\theta_{ijk}, \tilde{h}_{ijk}) = \theta_{ijk}\tilde{h}_{ijk} \tag{2}$$

where the path-loss θ_{ijk} is a function of the relative distance between the i-th UAV and the j-th user of group k and can be written as

$$\theta_{ijk} = d_{ijk}^{-n} = \theta_0 \sqrt{(x_{jk}-x_i)^2 + (y_{jk}-y_i)^2 + H^2}^{-n} \tag{3}$$

where $n > 2$ is the path loss exponent, and θ_0 is the path loss at a reference distance 1 m. We assume $\tilde{h}_{ijk}$ follows a K-factor Rician distribution ($K > 0$). Hence, $\tilde{h}_{ijk}$ is composed of a deterministic component $\bar{h}_{ijk}$ ($\left|\bar{h}_{ijk}\right| = 1$), and a random scattering component $\hat{h}_{ijk}$ following a complex Gaussian distribution $\mathscr{CN}(0,1)$. The small-scale fading coefficient $\tilde{h}_{ijk}$ is given by

$$\tilde{h}_{ijk} = \sqrt{\frac{K}{1+K}}\bar{h}_{ijk} + \sqrt{\frac{1}{1+K}}\hat{h}_{ijk} \tag{4}$$

D. Achievable rate analysis

We denote $s_k, \forall k \in \mathscr{K}$ as the signal with unit power, i.e., $\mathbb{E}\{s_k s_k^*\} = 1$ intended for the user group requesting c_k, $\mathbf{w}_k = [w_{1k}, w_{2k}, ..., w_{Uk}]^\intercal, \forall k \in \mathscr{K}$ as the beamforming vector from the U UAVs to the jth users of group k and $\mathbf{h}_{jk}(\theta_{jk}, \tilde{\mathbf{h}}_{jk}) = \left[h_{1jk}(\theta_{1jk}, \tilde{h}_{ijk}), \ldots, h_{Ujk}(\theta_{Ujk}, \tilde{h}_{ijk})\right]^\intercal$ as the vector that concatenates all the channels from U UAVs. To decide whether content k is placed in the i-th UAV, we introduce the binary variable $b_{ik}, \forall k \in \mathscr{K}, \forall j \in \mathscr{N}_k$. In particular, $b_{ik} = 1$ enforces that content k is stored in the i-th UAV and $b_{ik} = 0$ otherwise. Obviously, $b_{ik} = 0$ means the i-th UAV does not hold the content k and is therefore not able to cooperatively serve the users requesting content k. Thus, this UAV does not allocate any resource to these users. In other words, the beamforming applied on these users from i-th UAV is 0. Similarly, we denote $\mathbf{b}_k = [b_{1k}, b_{2k}, ..., b_{Uk}]^\intercal$ and $\mathbf{b} = \{\mathbf{b}_k, \forall k \in \mathscr{K}\}$ for notational convenience. Thus, the received signal at the j-th user of group k is writen as

$$y_{jk} = \mathbf{h}_{jk}(\theta_{jk}, \tilde{\mathbf{h}}_{jk})^\dagger (\mathbf{w}_k \circ \mathbf{b}_k) s_k + \sum_{\ell \neq k} \mathbf{h}_{jk}(\theta_{jk}, \tilde{\mathbf{h}}_{jk})^\dagger (\mathbf{w}_\ell \circ \mathbf{b}_\ell) s_l + n_{jk} \tag{5}$$

In (5), the first term is the signal of interest at the j-th user of group k, while the second term is the interfering signals (intended for the user requesting different contents) and $n_{jk} \sim \mathscr{CN}(0, \sigma_0^2)$ is the additive white Gaussian Noise (AWGN). For notational convenience, we denote $\mathbf{w} = \{\mathbf{w}_k, \forall k \in \mathscr{K}\}$ and $\theta = \{\theta_{jk}, \forall k \in \mathscr{K}, \forall j \in \mathscr{N}_k\}$. Given the above assumption, the signal-to-interference-plus-noise ratio at the j-th user of group k is written as

$$\Gamma_{jk}(\mathbf{w}, \theta, \tilde{\mathbf{h}}_{jk}, \mathbf{b}) = \frac{\left|(\mathbf{h}_{jk}(\theta_{jk}, \tilde{\mathbf{h}}_{jk}))^\dagger (\mathbf{w}_k \circ \mathbf{b}_k)\right|^2}{\sum_{\ell \neq k} \left|(\mathbf{h}_{jk}(\theta_{jk}, \tilde{\mathbf{h}}_{jk}))^\dagger (\mathbf{w}_\ell \circ \mathbf{b}_\ell)\right|^2 + \sigma_0^2} \tag{6}$$

Then, by treating interference as noise, the achievable rate in bps/Hz at the user is

$$R_{jk}(\mathbf{w}, \theta, \tilde{\mathbf{h}}_{jk}, \mathbf{b}) = \log(1 + \Gamma_{jk}(\mathbf{w}, \theta, \tilde{\mathbf{h}}_{jk}\mathbf{b})) \tag{7}$$

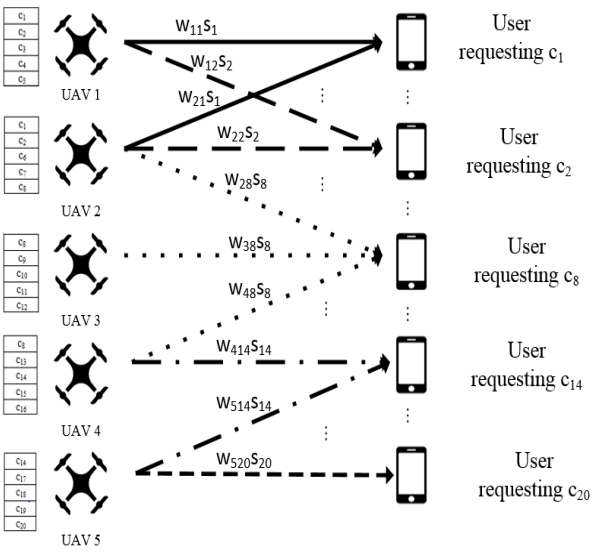

Fig. 2. An illustration for cooperative transmission of UAVs with limited storage capacity

To highlight the benefits of cooperative communication amongst limited-storage UAVs, let us perform some analysis on the following example:

An illustration for cooperative transmission design for limited-storage UAVs: In Fig. 2, we consider a system of 5 UAVs and a group of ground users requesting 20 different contents that are randomly distributed in the service region. We assume there are 20 contents to be requested by the users and the storage space at each UAV is 5 contents. The contents are loaded on each UAV and then the UAVs are dispatched to serve ground users. Note that in this example, although we assume a random content placement scheme for ease of illustration, a more strategic content placement is determined via the optimization problem we introduce later. The UAVs are able to serve the users via beamforming. Since the total storage space is 25, some UAVs can accommodate copies of the same contents and therefore can cooperate with each other to serve ground users. In Fig. 2, UAVs 1 and 2 store the same contents c_1 and c_2 and can support each other to serve the users requesting these file via a proper design of the weights w_{11}, w_{12}, w_{21}, w_{22}. Similarly, UAVs 2, 3 and 4 all store the content c_8 and thus can cooperate to serve users requesting it. The cooperation rule remains the same for UAVs 4 and 5. Since users requesting the duplicate contents stored in multiple UAVs benefit from the cooperation, the overall network performance is improved.

III. Problem Formulation

A. Formulation approach

Before formulating the problem, it is worth noting that the rate function is constituted by the channel coefficient $h_{ijk}(\theta_{ijk}, \tilde{h}_{ijk})$. However, the small-scale fading $\tilde{h}_{ijk}$ is a random complex number and is impossible to obtain prior to the deployment of UAVs. Without a deterministic value of small-scale fading, formulation of joint beamforming and location optimization cannot be done. Thus, our proposed approach is

This article has been accepted for publication in a future issue of this journal, but has not been fully edited. Content may change prior to final publication. Citation information: DOI 10.1109/TCOMM.2019.2936354, IEEE Transactions on Communications

first considering the AtG channels are composed of the path loss only. In other words, we initially neglect the impact of small-scale fading and rewrite (2), (6), and (7) as functions of merely path loss as follows.

$$h_{ijk}(\theta_{ijk}) = \theta_{ijk} \tag{8}$$

$$\Gamma_{jk}(\mathbf{w},\theta,\mathbf{b}) = \frac{\left|(\mathbf{h}_{jk}(\theta_{jk}))^{\dagger}(\mathbf{w}_k \circ \mathbf{b}_k)\right|^2}{\sum\limits_{\ell\neq k}\left|(\mathbf{h}_{jk}(\theta_{jk}))^{\dagger}(\mathbf{w}_\ell \circ \mathbf{b}_\ell)\right|^2 + \sigma_0^2} \tag{9}$$

$$R_{jk}(\mathbf{w},\theta,\mathbf{b}) = \log(1+\Gamma_{jk}(\mathbf{w},\theta,\mathbf{b})) \tag{10}$$

With the deterministic form of the rate function (10), we can proceed to formulate the user admission maximization problem. Then, after solving the first problem, we can obtain the solution for user admission decision, content placement, beamforming and UAVs' locations. However, when deploying UAVs following the obtained solution, the rate quality may degrade with the existence of small-scale fading. To mitigate this potential rate loss, we introduce another supplement problem to adjust the beamformers in each channel realization. The two formulated problems are introduced subsequently. Note that although this approach is heuristic, the rate loss is insignificant when the UAVs' altitude is large since the path loss component would be the dominant factor ($K >> 1$ and $|\tilde{h}_{ijk}| \approx 1$).

B. User admission maximization

We first start with the user admission maximization problem. Let us introduce the admission decision variable $\mathbf{a} = \left\{a_{jk}, \forall j \in \mathcal{N}_k, \forall k \in \mathcal{K}\right\}$, where $a_{jk} = \{0,1\}$. $a_{jk} = 1$ enforces that the j-th user belonging to group k is admitted, and $a_{jk} = 0$ otherwise. The rate quality at each user depends on the beamforming vectors and path loss (or the UAVs' positions). Besides, the admission decision and the content placement, which influence the beamforming design, also affect the rate quality. As a result, our user admission maximization problem can be written as follows

$$\max_{\mathbf{a},\mathbf{b},\mathbf{w},\theta,\mathbf{p}} \quad \sum_{k\in\mathcal{K}}\sum_{j\in\mathcal{N}_k} a_{jk} \tag{11a}$$

$$\text{s.t.} \quad R_{jk}(\mathbf{w},\theta,\mathbf{b}) \geq a_{jk} R^k_{\min}, \forall j \in \mathcal{N}_k, \forall k \in \mathcal{K} \tag{11b}$$

$$\sum_{k\in\mathcal{K}} |\, b_{ik} w_{ik} \,|^2 \leq P_{\max}, \forall i \in \mathcal{U} \tag{11c}$$

$$a_{jk} = \{0,1\}, \forall j \in \mathcal{N}_k, \forall k \in \mathcal{K} \tag{11d}$$

$$b_{ik} = \{0,1\}, \forall i \in \mathcal{U}, \forall k \in \mathcal{K} \tag{11e}$$

$$\sum_{k\in\mathcal{K}} b_{ik} \leq S, \forall i \in \mathcal{U} \tag{11f}$$

$$\theta_{ijk}^{-1/n} \geq \tilde{\theta}_0 \sqrt{(x_{jk}-x_i)^2 + (y_{jk}-y_i)^2 + H^2}, \forall i \in \mathcal{U}, \forall j \in \mathcal{N}_k, \forall k \in \mathcal{K} \tag{11g}$$

where constraint (11b) ensures a minimum rate for the admitted users, constraint (11c) presents the maximum power budget for each UAV, constraint (11f) implies that the total number of contents on each UAV should not exceed a maximum storage capacity S, constraint (11g) presents the relationship between the path loss and the UAV's position. It is noted that constraint (11g) is active and equivalent to (3) at the optimality for problem (11). Proof of this claim is similar to Appendix I in [34].

C. QoS maximization

After solving problem (11), the UAVs are deployed following the obtained optimal value $\mathbf{a}^* = \left\{a^*_{jk}, \forall j \in \mathcal{N}_k, \forall k \in \mathcal{K}\right\}$, content placement $\mathbf{b}^* = \left\{b^*_{ik}, \forall i \in \mathcal{U}, \forall k \in \mathcal{K}\right\}$, and UAVs' positions $\mathbf{p}^* = \{\mathbf{p}^*_i, \forall i \in \mathcal{U}\}$. However, with the presence of small-scale fading after deployment, the minimum required rate $R^k_{\min}$ may sometimes not be satisfied. Hence, the beamforming vectors can be adjusted at each channel realization according to the actual small-scale fading information, which can be obtained via pilot sequences. Let us denote $\mathbf{w}_n$ as the beamforming vectors at channel realization n, we introduce the following problem

$$\max_{\mathbf{w}_n} \quad \sum_{k\in\mathcal{K}}\sum_{j\in\mathcal{N}_k} R_{jk}(\mathbf{w}_n) \tag{12a}$$

$$\text{s.t.} \quad R_{jk}(\mathbf{w}_n) \geq a^*_{jk} \bar{R}^k_{\min}, \forall j \in \mathcal{N}_k, \forall k \in \mathcal{K} \tag{12b}$$

$$\sum_{k\in\mathcal{K}} |\, b^*_{ik} w_{ik,n} \,|^2 \leq P_{\max}, \forall i \in \mathcal{U} \tag{12c}$$

The purpose of problem (12) is to enhance the data rate at the admitted user by adjusting the beamforming $\mathbf{w}_n$ based on the instantaneous channel state information (CSI) $h_{ijk,n}(\theta_{ijk}, \tilde{h}_{ijk,n}) = \theta_{ijk}\tilde{h}_{ijk,n}$. However, problem (12) may sometimes be infeasible if the small-scale fading is severe. A countermeasure is to offset $R^k_{\min}$ in the initial problem by a small value χ^k, i.e., $R^k_{\min} = \bar{R}^k_{\min} + \chi^k$. For instance, if the actual target QoS requirement is 0.5 bps/Hz, we can set $R^k_{\min} = 0.55$ and $\chi^k = 0.05$. The value χ^k will depend on the Rician factor K, which presents the dominance of LoS components in the channel.

IV. Solution Approach

First, we deal with problem (11). We propose the following equivalent transformation for problem (11) as follows

$$\max_{\substack{\mathbf{a},\mathbf{b},\mathbf{w},\\ \lambda,\theta,\mathbf{p}}} \quad \sum_{k\in\mathcal{K}}\sum_{j\in\mathcal{N}_k} a_{jk} \tag{13a}$$

$$\text{s.t.} \quad R_{jk}(\mathbf{w},\theta) \geq a_{jk} R^k_{\min}, \forall j \in \mathcal{N}_k, \forall k \in \mathcal{K} \tag{13b}$$

$$|\, w_{ik} \,|^2 \leq b_{ik}\lambda_{ik}, \forall i \in \mathcal{U}, \forall k \in \mathcal{K} \tag{13c}$$

$$\sum_{k\in\mathcal{K}} \lambda_{ik} \leq P_{\max}, \forall i \in \mathcal{U} \tag{13d}$$

$$(11d) - (11g)$$

Here, we introduce two new constraints (13c) and (13d) as a replacement for constraint (11c) to free the variables $\mathbf{b}$ from the rate function. Thus, the new rate function in (13b) can be written as $R_{jk}(\mathbf{w},\theta) = \log(1+\Gamma_{jk}(\mathbf{w},\theta))$ where $\Gamma_{jk}(\mathbf{w},\theta) = \frac{\left|(\mathbf{h}_{jk}(\theta_{jk}))^{\dagger}\mathbf{w}_k\right|^2}{\sum\limits_{\ell\neq k}\left|(\mathbf{h}_{jk}(\theta_{jk}))^{\dagger}\mathbf{w}_\ell\right|^2 + \sigma_0^2}$. It is worth noting that we also introduce a new variable $\lambda = \{\lambda_{ik}, \forall i \in \mathcal{U}, \forall k \in \mathcal{K}\}$ that indicates the soft-power level that the UAVs applied on the user group k (the optimized power when the binary variable b_{ik} is relaxed to continuous value). The constraints (13c) and (13d) convey the same meaning as constraint (11c). The reason behind our transformation is to smoothen the achievable rate function by

This article has been accepted for publication in a future issue of this journal, but has not been fully edited. Content may change prior to final publication. Citation information: DOI 10.1109/TCOMM.2019.2936354, IEEE Transactions on Communications

removing the variable $\mathbf{b}$ as well as the dot-product operation. Since the new rate function, i.e., $R_{jk}(\mathbf{w},\theta)$, is now a smooth function, our later introduced DC-based approximation, which requires the derivation of gradient vectors, can be applied.

V. Low-complexity Algorithm

First and foremost, we acknowledge that problem (13) is non-convex because of the non-convexity of constraints (13b), (13c), (11g). In this section, we propose an algorithm developed on the basis of DC-programming and successive convex approximation (SCA) [35]. Since the rate function $R_{jk}(\mathbf{w},\theta)$ is not inherently presented as a difference of two convex functions, so-called a DC function. We first apply DC decomposition to turn it into a DC form.

A. DC decomposition

$R_{jk}(\mathbf{w},\theta)$ can be written as

$$\underbrace{R_{jk}(\mathbf{w},\theta)+\xi_{jk}(\|\mathbf{w}\|^2+\|\theta\|^2)}_{f_{jk}(\mathbf{w},\theta)}-\xi_{jk}(\|\mathbf{w}\|^2+\|\theta\|^2)$$

An important observation is that if the parameter $\xi_{jk}>0$ is sufficiently large, function $f_{jk}(\mathbf{w},\theta)$ becomes convex with respect to $\mathbf{w}$ and θ due to the dominance of the strongly convex component $\xi_{jk}(\|\mathbf{w}\|^2+\|\theta\|^2)$. Consequently, function $R_{jk}(\mathbf{w},\theta)$ turns into a DC function. Thus, we introduce the following theorem.

Theorem 1. *For $\xi_{jk}\geq\xi_0$, where ξ_0 is derived in Appendix A, $f_{jk}(\mathbf{w},\theta)$ is strongly convex and $R_{jk}(\mathbf{w},\theta)$ becomes a DC function.*

Proof: Please refer to Appendix A. □

After applying the above decomposition, we can rewrite problem (13) as

$$\max_{\substack{\mathbf{a},\mathbf{b},\mathbf{w},\\ \lambda,\theta,\mathbf{p}}} \quad \sum_{j\in\mathcal{N}_k}\sum_{k\in\mathcal{K}} a_{jk} \tag{14a}$$

$$\text{s.t.} \quad f_{jk}(\mathbf{w},\theta)-\xi_{jk}(\|\mathbf{w}\|^2+\|\theta\|^2)\geq a_{jk}R^k_{\min},\forall j\in\mathcal{N}_k,\forall k\in\mathcal{K} \tag{14b}$$

$$(11c)-(11g)$$

The left-hand side (LHS) of constraint (14b) now has DC form. Next, we introduce the DC-based approximation framework.

B. The DC-based approximation method

To describe the method, let us revisit the following DC-form constraint

$$f(\mathbf{x})-g(\mathbf{x})\geq 0 \tag{15}$$

where $f(\mathbf{x})$ and $g(\mathbf{x})$ are both convex with respect to variable $\mathbf{x}$. Note that in order for constraint (15) to characterize a feasible convex set, its left-hand side must be a concave function. Hence, the convex function $f(\mathbf{x})$ is the reason why constraint (15) is not convex. Assuming that $f(\mathbf{x})$ is differentiable, the first step of DC-based method is the linear approximation of $f(\mathbf{x})$ around the point $\mathbf{x}^{[\ell]}$ to convexify (15) into the following constraint

$$f_{\mathscr{T}}(\mathbf{x}^{[\ell]})-g(\mathbf{x})\geq 0 \tag{16}$$

(16) replaces $f(\mathbf{x})$ with its lower-bound first-order Taylor approximation $f_{\mathscr{T}}(\mathbf{x}^{[\ell]})$ around point $\mathbf{x}^{[\ell]}$. Hence, optimization problems with constraints following the form of (15) can be solved by iterative relaxation of non-convex constraints (15) into a convex approximation form as in (16). To apply this principle in our problem, we first acknowledge that problem (20) is nonconvex because of the convex function $f_{jk}(\mathbf{w},\theta)$ (with a sufficiently large value of ξ_{jk}) on the greater side of constraint (14b). Thus, we replace it by its first-order Taylor approximation $F_{jk}(\mathbf{w},\theta)$ around point $\mathbf{w}^{[\ell]}$ and $\theta^{[\ell]}$ as follows

$$\begin{aligned}&F_{jk}(\mathbf{w},\theta;\mathbf{w}^{[\ell]},\theta^{[\ell]})=\\ &f_{jk}(\mathbf{w}^{[\ell]},\theta^{[\ell]})+\underbrace{\hat{f}_{jk}(\mathbf{w};\mathbf{w}^{[\ell]},\theta^{[\ell]})+\check{f}_{jk}(\theta;\mathbf{w}^{[\ell]},\theta^{[\ell]})}_{\tilde{F}(\mathbf{w},\theta;\mathbf{w}^{[l]},\theta^{[\ell]})}-\\ &\underbrace{2\xi_{jk}\,\mathrm{Re}\left((\mathbf{w}^{[\ell]})^\dagger\mathbf{w}-\left\|\mathbf{w}^{[\ell]}\right\|^2+(\theta^{[\ell]})^\dagger\theta-\left\|\theta^{[\ell]}\right\|^2\right)}_{\bar{F}(\mathbf{w},\theta;\mathbf{w}^{[\ell]},\theta^{[\ell]})}\end{aligned} \tag{17}$$

where

$$\begin{aligned}&\hat{f}_{jk}(\mathbf{w};\mathbf{w}^{[\ell]},\theta^{[\ell]})=\\ &\frac{2\mathrm{Re}\left((\mathbf{w}^{[\ell]})^\dagger\mathbf{H}_{jk}\left(\theta^{[\ell]}\right)\mathbf{w}-(\mathbf{w}^{[\ell]})^\dagger\mathbf{H}_{jk}\left(\theta^{[\ell]}\right)\mathbf{w}^{[\ell]}\right)}{(\mathbf{w}^{[\ell]})^\dagger\mathbf{H}_{jk}\left(\theta^{[\ell]}\right)\mathbf{w}^{[\ell]}+\sigma_0^2}-\\ &\frac{2\mathrm{Re}\left((\mathbf{w}^{[\ell]})^\dagger\tilde{\mathbf{H}}_{jk}\left(\theta^{[\ell]}\right)\mathbf{w}-(\mathbf{w}^{[\ell]})^\dagger\tilde{\mathbf{H}}_{jk}\left(\theta^{[\ell]}\right)\mathbf{w}^{[\ell]}\right)}{(\mathbf{w}^{[\ell]})^\dagger\tilde{\mathbf{H}}_{jk}\left(\theta^{[\ell]}\right)\mathbf{w}^{[\ell]}+\sigma_0^2},\end{aligned} \tag{18}$$

and

$$\begin{aligned}&\check{f}_{jk}(\theta;\mathbf{w}^{[\ell]},\theta^{[\ell]})=\\ &\frac{2\mathrm{Re}\left((\theta^{[l]})^\dagger\Omega_{jk}\left(\mathbf{w}^{[\ell]}\right)\theta-(\theta^{[\ell]})^\dagger\Omega_{jk}\left(\mathbf{w}^{[\ell]}\right)\theta^{[l]}\right)}{(\mathbf{w}^{[\ell]})^\dagger\Omega_{jk}\left(\theta^{[\ell]}\right)\mathbf{w}^{[\ell]}+\sigma_0^2}-\\ &\frac{2\mathrm{Re}\left((\theta^{[\ell]})^\dagger\tilde{\Omega}_{jk}\left(\mathbf{w}^{[\ell]}\right)\theta-(\theta^{[\ell]})^\dagger\tilde{\Omega}_{jk}\left(\mathbf{w}^{[\ell]}\right)\theta^{[\ell]}\right)}{(\mathbf{w}^{[\ell]})^\dagger\tilde{\Omega}_{jk}\left(\theta^{[\ell]}\right)\mathbf{w}^{[\ell]}+\sigma_0^2},\end{aligned} \tag{19}$$

The derivation of $\mathbf{H}_{jk}$, $\tilde{\mathbf{H}}_{jk}$, Ω_{jk}, and $\tilde{\Omega}_{jk}$ are in presented in Appendix A. After applying DC-based approximation, we obtain the following optimization problem

$$\max_{\substack{\mathbf{a},\mathbf{b},\mathbf{w},\\ \lambda,\theta,\mathbf{p}}} \quad \sum_{j\in\mathcal{N}_k}\sum_{k\in\mathcal{K}} a_{jk} \tag{20a}$$

$$\begin{aligned}\text{s.t.}\quad &F_{jk}(\mathbf{w},\theta;\mathbf{w}^{[\ell]},\theta^{[\ell]})-\xi_{jk}(\|\mathbf{w}\|^2+\|\theta\|^2)\\ &\geq a_{jk}R^k_{\min},\forall j\in\mathcal{N}_k,\forall k\in\mathcal{K}\\ &(13c),(13d),(11d)-(11g)\end{aligned} \tag{20b}$$

The above problem is still non-convex due to non-convex constraints (13c) and (11g) and the variables $\mathbf{a}$, $\mathbf{b}$. The tackle this, transformations and relaxations of these constraints need to be applied.

This article has been accepted for publication in a future issue of this journal, but has not been fully edited. Content may change prior to final publication. Citation information: DOI 10.1109/TCOMM.2019.2936354, IEEE Transactions on Communications

C. Constraint transformation and relaxation.

First, we relax the binary variables $\mathbf{a}$ and $\mathbf{b}$ into continuous and replace (11d) and (11e) with the following constraints while still maintaining the equivalence

$$a_{jk} - a_{jk}^2 \leq 0 \tag{21}$$
$$0 \leq a_{jk} \leq 1 \tag{22}$$
$$b_{ik} - b_{ik}^2 \leq 0 \tag{23}$$
$$0 \leq b_{ik} \leq 1 \tag{24}$$

Since (21) and (23) are non-convex constraints, we replace the left-hand sides of them by their upper-bound first-order Taylor approximation around points $a_{jk}^{[\ell]}$ and $b_{jk}^{[\ell]}$ as follows

$$a_{jk} - (a_{jk}^{[\ell]})^2 - 2(a_{jk}^{[\ell]} a_{jk} - (a_{jk}^{[\ell]})^2) \leq 0 \tag{25}$$
$$b_{ik} - (b_{ik}^{[\ell]})^2 - 2(b_{ik}^{[\ell]} a_{ik,t} - (b_{ik}^{[\ell]})^2) \leq 0 \tag{26}$$

Thanks to the work [36], we acknowledge that the above constraints can render our DC-based iterative algorithm unable to compute a feasible solution when coupled with constraints (21) and (23). We make sure $a_{jk}^{[\ell]}$ and $b_{ik}^{[\ell]}$ are always feasible by introducing two slack variables μ_{jk} and ν_{ik} as follows

$$a_{jk} - (a_{jk}^{[\ell]})^2 - 2(a_{jk}^{[\ell]} a_{jk} - (a_{jk}^{[\ell]})^2) \leq \mu_{jk} \tag{27}$$
$$b_{ik} - (b_{ik}^{[\ell]})^2 - 2(b_{ik}^{[\ell]} b_{ik,t} - (b_{ik}^{[\ell]})^2) \leq \nu_{ik} \tag{28}$$

To maintain the equivalence of our problem, the variables μ_{jk} and ν_{ik}, associated with some penalty parameters, are deducted to the objective function and the optimality of the problem occurs when μ_{jk} and ν_{ik} approach 0.

Next, by simple algebraic manipulation, we can transform the constraint (13c) into the following

$$\sqrt{|\, w_{ik} \,|^2 + \frac{(b_{ik} - \lambda_{ik})^2}{4}} \leq \frac{b_{ik} + \lambda_{ik}}{2} \tag{29}$$

After the manipulation, it is obvious that (29) is the second-order cone representation of constraint (13c). Finally, to deal with constraint (11g), we replace the left-hand side by its lower-bound first-order Taylor approximation around point $\theta_{ijk}^{[\ell]}$ as follows

$$\theta_{ijk}^{[\ell]} - \frac{1}{\alpha} \theta^{\frac{-1-n}{n}} (\theta - \theta^{[\ell]}) \geq \tilde{\theta}_0 \sqrt{(x_{jk} - x_i)^2 + (y_{jk} - y_i)^2 + H^2} \tag{30}$$

Let us denote $\tilde{\mathbf{M}} = \{\mu_{jk}, \forall j \in \mathcal{N}_k, \forall k \in \mathcal{K}\}$, $\tilde{\mathbf{N}} = \{\nu_{ik}, \forall i \in \mathcal{U}, \forall k \in \mathcal{K}\}$. By applying the above relaxation and approximation, we obtain a convex optimization problem at the ℓ-th iteration

$$\max_{\substack{\mathbf{a},\mathbf{b},\mathbf{w},\\ \boldsymbol{\lambda},\theta,\mathbf{p}}} \quad \sum_{k\in\mathcal{K}} \sum_{j\in\mathcal{N}_k} a_{jk} - M^{[\ell]} \sum_{k\in\mathcal{K}} \sum_{j\in\mathcal{N}_k} \mu_{jk} - N^{[\ell]} \sum_{k\in\mathcal{K}} \sum_{i\in\mathcal{U}} \nu_{ik} \tag{31a}$$

$$\text{s.t.} \quad F_{jk}(\mathbf{w}, \theta; \mathbf{w}^{[\ell]}, \theta^{[\ell]}) - \xi_{jk}(\|\mathbf{w}\|^2 + \|\theta\|^2) \geq a_{jk} R_{\min}^k, \forall j \in \mathcal{N}_k \tag{31b}$$

$$\sum_{k\in\mathcal{K}} b_{ik} \leq S, \forall i \in \mathcal{U} \tag{31c}$$

$$\sqrt{|\, w_{ik} \,|^2 + \frac{(b_{ik} - \lambda_{ik})^2}{4}} \leq \frac{b_{ik} + \lambda_{ik}}{2}, \forall k \in \mathcal{K}, \forall i \in \mathcal{U} \tag{31d}$$

$$\sum_{k\in\mathcal{K}} \lambda_{ik} \leq P_{\max}, \forall i \in \mathcal{U} \tag{31e}$$

$$0 \leq a_{jk} \leq 1, \forall j \in \mathcal{N}_k, \forall k \in \mathcal{K} \tag{31f}$$

$$a_{jk} - (a_{jk}^{[\ell]})^2 - 2(a_{jk}^{[\ell]} a_{jk} - (a_{jk}^{[\ell]})^2) \leq \mu_{jk}, \forall j \in \mathcal{N}_k, \forall k \in \mathcal{K} \tag{31g}$$

$$0 \leq b_{jk,t} \leq 1, \forall i \in \mathcal{U}, \forall k \in \mathcal{K} \tag{31h}$$

$$b_{ik} - (b_{ik}^{[\ell]})^2 - 2(b_{ik}^{[\ell]} b_{ik,t} - (b_{ik}^{[\ell]})^2) \leq \nu_{ik}, \forall i \in \mathcal{U}, \forall k \in \mathcal{K} \tag{31i}$$

(31j)

$$\theta_{ijk}^{[\ell]} - \frac{1}{\alpha} \theta^{(-1-n)/n} (\theta - \theta^{[\ell]}) \geq \tilde{\theta}_0 \sqrt{(x_{jk} - x_i)^2 + (y_{jk} - y_i)^2 + H^2}, \forall j \in \mathcal{N}_k, \forall k \in \mathcal{K} \tag{31k}$$

Note that in problem (31) the slack variables μ_{jk} and ν_{ik}, coupled with the penalty parameters $M^{[\ell]}$ and $N^{[\ell]}$, have been deducted from the original objective function. It is obvious that when μ_{jk} and ν_{ik} approach 0, the variables a_{jk} and b_{ik} converge to either 0 or 1. The values $M^{[\ell]}$ and $N^{[\ell]}$ are initiated at some small positive values and are updated by multiplying with values $\varepsilon_M, \varepsilon_N > 1$ to ensure that $\sum_{k\in\mathcal{K}} \sum_{j\in\mathcal{N}_k} \mu_{jk}$ and $\sum_{k\in\mathcal{K}} \sum_{i\in\mathcal{U}} \nu_{ik}$ approach 0 when $M^{[\ell]}$ and $N^{[\ell]}$ approach some large values $M_{\max}$ and $N_{\max}$.

At the ℓ-th iteration, the initial mixed-integer non-convex problem (11) has been approximated into a continuous second-order cone program (SOCP), which can be handled by modern optimization solvers [37]. Thus, the SCA method, which is widely known in the wireless communication and signal processing community, can be applied. Algorithm 1 outlines our method to solve problem (11). After solving problem (11),

Algorithm 1 DC-based SCA method

1: Initialize starting values of $\mathbf{a}^{[\ell]}$, $\mathbf{b}^{[\ell]}$, $\mathbf{w}^{[\ell]}$, $\theta^{[\ell]}$,$\mathbf{p}^{[\ell]}$, $M^{[\ell]}$, and $N^{[\ell]}$
2: Set $\ell := 0$;
3: **repeat**
4: Solve the convex problem (31) to obtain $\mathbf{a}^*$, $\mathbf{b}^*$, $\mathbf{w}^*$, θ^*,p^*;
5: Set $\ell := \ell + 1$;
6: Update $\mathbf{a}^{[\ell]} = \mathbf{a}^*$, $\mathbf{b}^{[\ell]} = \mathbf{b}^*$, $\mathbf{w}^{[\ell]} = \mathbf{w}^*$, $\theta^{[\ell]} = \theta^\star$,$\mathbf{p}^{[\ell]}$=$\mathbf{p}^*$;
7: Update $M^{[\ell]} = \min\{\varepsilon_M M^{[\ell-1]}, M_{\max}\}$ and $N^{[\ell]} = \min\{\varepsilon_N N^{[\ell-1]}, N_{\max}\}$;
8: **until** Convergence of the objective function (31a); $\mathbf{a}^* = \mathbf{a}^{[\ell]}$, $\mathbf{b}^* = \mathbf{b}^{[\ell]}$, $\mathbf{w}^* = \mathbf{w}^{[\ell]}$, $\theta^* = \theta^{[\ell]}$,$\mathbf{p}^* = \mathbf{p}^{[\ell]}$

values $\mathbf{a}^*$, $\mathbf{b}^*$,$\mathbf{p}^*$ can be used to proceed to solve problem (12). Since problem (12) is continuous and non-convex due to the function $R_{jk}(\mathbf{w}_n)$, we can apply DC decomposition and SCA the same as with function $R_{jk}(\mathbf{w}, \theta)$ in problem (11) (θ is a now constant since we know p^*).

VI. Numerical Results and Discussion

In this section, we present numerical results to evaluate the performance of our proposed scheme and draw some

This article has been accepted for publication in a future issue of this journal, but has not been fully edited. Content may change prior to final publication. Citation information: DOI 10.1109/TCOMM.2019.2936354, IEEE Transactions on Communications

engineering insights from adjusting the system parameters. We also compare our scheme with non-cooperative power allocation scheme [27] and joint beamforming [31]. We first solve problem (11) with a value $R^k_{\min}$ greater than the actual minimum required rate $\bar{R}^k_{\min}$. Then, problem (13) is solved with value $\bar{R}^k_{\min}$ to determine the optimal beamforming at each channel realization. However, it is noted that $\bar{R}^k_{\min}$ and $R^k_{\min}$ can be roughly the same, especially when the Rician factor K is large.

Settings: we consider a wireless communication system with a circular coverage of radius $r = 100$ m. There are 20 ground users that are randomly distributed within the circle. These users request 6 different contents whose request probability follow the Zipf distribution. Unless otherwise stated, $\theta_0 = -50$ dB, n=2.3 , K= 12 dB, S=3, $U = 6$, $H = 100$ m and $\alpha = 0.6$. We assume the flexible LTE bandwidth of $W = 20$ MHz [38]. Thus, the AWGN noise power is $\sigma_0^2 = -174 + 10\log(W) \approx -100$ dBm since the UAVs are operating on the whole available bandwidth. The number of admitted users is averaged out over 100 randomly generated small-scale fading and user distributions and is rounded to the nearest integer. Note that although the users' QoS requirements are usually different from each other in practice, we consider the same minimum QoS requirement for all users for the sake of fair evaluation. For instance, if we set the requirement of a user group very low and the others very high, the system may only admit the group with the lower requirements and rejects the others despite varying the parameters.

In Fig. 3, we investigate the system performance under five scenarios with different (minimum) QoS requirements. Specifically, the QoS requirements, i.e., $\bar{R}^k_{\min}$, in scenarios 1, 2, 3, 4 and 5 is 0.1, 0.2, 0.4, 0.6 and 0.8 bps/Hz, respectively. Note that the QoS requirements have been normalized by W and the bitrate (in bps) is $W\bar{R}^k_{\min}$. Thus, the users admitted in scenarios 1, 2, 3, 4 and 5 can experience the bitrates 2, 4, 8, 12, and 16 Mbps, respectively. These bitrates can provide high-quality videos. For instance, the bitrates in scenarios 2, 3 and 4 are higher than the required rates for 480p, 720p and 1080p video quality, respectively [39].[3] As illustrated, the more we increase the minimum rate requirements, the fewer users the system can admit considering the same power budget. We also notice that the number of admitted users can be 0 when the power budget is low. The reason is the effect of path loss caused by the high-altitude deployment of UAVs makes the received signal very weak. In addition, increasing the power budget on UAVs leads to minor improvements on user admission as the QoS requirements become higher. For example, in scenario 5, no user is admitted at 18 dBm and only 3 are admitted at 28 dBm, which is 10-time higher power consumption. This is due to the following reasons. First, the received signals at the users experience significant path loss due to the UAVs' altitude and their own distance from the users. We will later show that increasing the number of UAVs can mitigate this trend since the UAVs can move closer to the users, especially those at the edge. Second, when the UAVs cannot support more users given their power budget, the power is reserved to increase the rate of the admitted users due to problem (13).

[3]The redundant bandwidth can be reserved for cyclic prefix, signaling overhead, and pilot overhead.

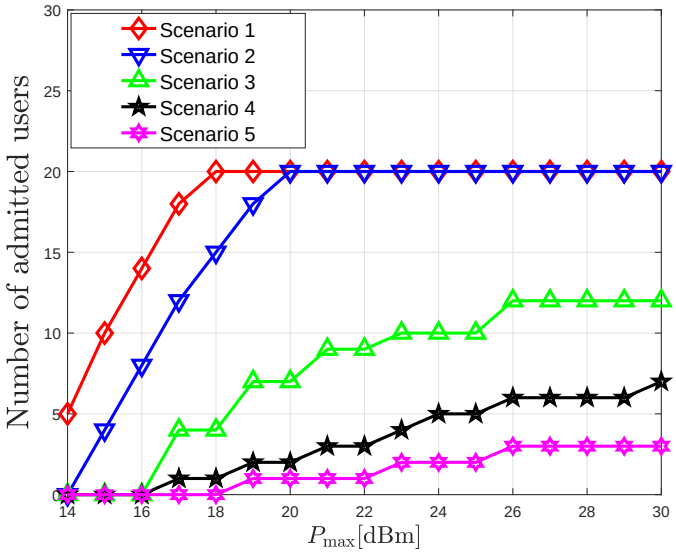

Fig. 3. Number of admitted users versus the maximum power budget per UAV with different QoS requirements

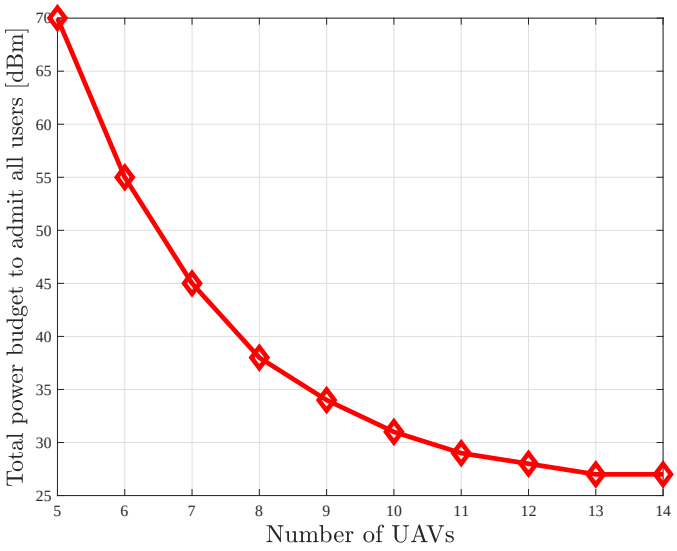

Fig. 4. Minimum total power budget to admit all users versus different numbers of cooperative UAVs.

As demonstrated in Fig. 3, increasing power is inefficient to enhance user admission. Thus, in Fig. 4, we increase the number of UAVs and see what is the minimum overall power budget (which is divided equally to each UAV) to admit all 20 users in each case. The QoS requirement is the same as Scenario 3 in Fig. 3. It is worth mentioning that the power budget in Fig. 4 is unrealistically increased up approximately 68 dBm per UAVs (70 dBm in total) for the sole purpose of highlighting the relationship between the number of UAVs and the power needed to admit all users. Fig. 4 shows that by adding 5 UAVs, the required total power can be reduced by 40 dBm (10^4 times), which is very significant. This is due to the following reasons. First, increasing the number of UAVs

This article has been accepted for publication in a future issue of this journal, but has not been fully edited. Content may change prior to final publication. Citation information: DOI 10.1109/TCOMM.2019.2936354, IEEE Transactions on Communications

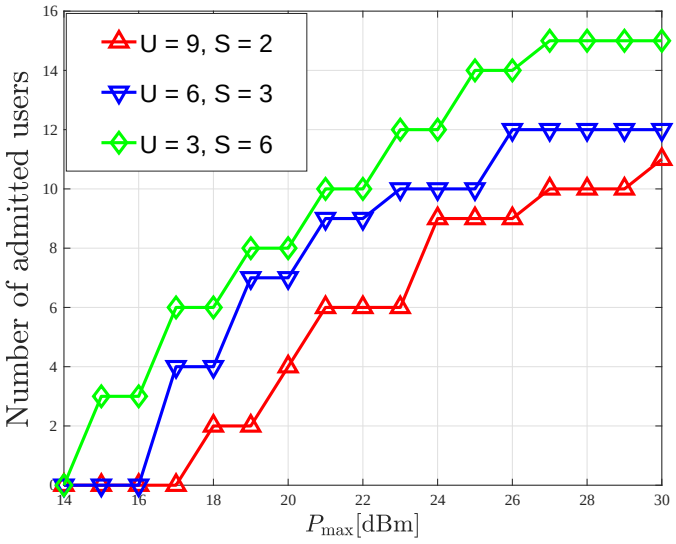

Fig. 5. Number of admitted users versus power budget per UAV with the same total storage space and different number of UAVs.

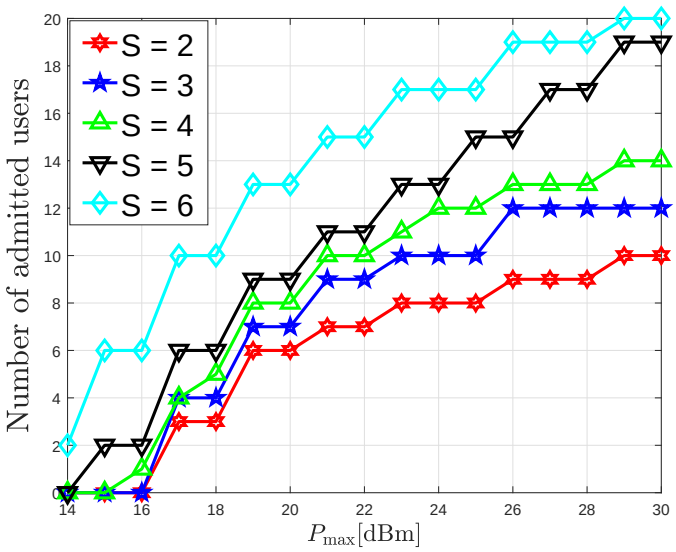

Fig. 6. Number of admitted users versus power budget per UAV with the same total storage space and different number of UAVs.

allows more UAVs to cooperate and boost received signal strength. Second, with more UAVs, each one has more freedom to fly closer to the users to significantly reduce the path loss. We also notice that this trend slows down gradually as we decrease the total power budget since after a certain point, the cooperation cannot overcome a fixed path-loss induced by the altitude $H = 100$ m when the overall power budget becomes too small. This observation offers a notable insight that more UAVs with lower power budget working in a cooperative manner consumes much less power than fewer UAVs high power to achieve the same user admission. Thus, employing more cooperative UAVs may to improve UAVs' lifetime.

In Fig. 5, we consider a fixed total storage capacity of 18 contents while deploying different numbers of UAVs. The QoS requirement is the same as Scenario 3 in Fig. 3. As illustrated, deploying more UAVs with lower storage capacity on each UAV results in higher user admission. Thus, when considered as a resource, storage capacity plays a similar role to power budget per UAVs. Thus, from a more general perspective, Overall, Fig. 4 and Fig. 5 reveal that UAVs with limited capability (in terms of payload and power) can cooperatively work together and still outperform UAVs with much higher capability.

In Fig. 6, we observe the effect of storage capacity on the system performance while keeping the number of UAVs unchanged. The QoS requirement is as in scenario 3 of Fig. 3. Similar to the impact of the number of UAVs, more storage capacity results in higher user admission. The reason is that when we have more storage capacity, more UAVs can store the duplicate versions of the same contents and thus increase the cooperation among UAVs.

In Fig. 7, we draw the comparison among different interference mitigation schemes. The QoS' requirements are as in scenario 3 of Fig. 3. In the power allocation scheme, each UAV is assigned to serve each user group. We optimized the power that each UAV allocates to its corresponding user group and the UAVs' positions so as to mitigate inter-group interference. Some drawbacks of the power allocation scheme are considering no cooperation among UAVs based on content storage and only taking into consideration the amplitude of the transmitted signal while neglecting the phase components. Thus, the power allocation scheme performs poorly when the users are scattered. For the joint beamforming scheme [31], we also employ beamforming and location optimization as in our scheme. However, in this case, all the UAVs serve all the users via joint transmissions. As demonstrated in Fig 4, the system performance is supposed to be enhanced when more UAVs can serve one user group. However, this is only true when we have enough storage to store most of the contents to be requested (ideally all contents). Since we are considering a practical scenario with limited storage capacity, the UAVs can only store the most popular contents and the number of admitted users is upper-bounded by the total number of users requesting these contents. As illustrated, our proposed scheme outperforms the others since we are considering signal-level coordination (beamforming), UAVs' locations, and strategic content placement with limited storage capacity per UAV simultaneously.

Fig. 8 shows the impact of different values of α in our system. The QoS requirements are as in scenario 3 of Fig. 3. The value α, which has been presented in section II-B, represents the degree that the content request distribution is concentrated on the most popular contents. In other words, the larger α, the larger the number of users requests the most common contents. As shown in Fig. 8, our system performance increases with α. Since there are more users requesting the most popular contents, it is more likely the contents are loaded in the UAVs as our objective is to maximize the number of served users. Thus, there are more copies of the same contents in the UAVs (constrained by the storage capacity), which enhances UAVs' cooperation. This trend has been referred to as higher *content reuse* in previous literature [40].

This article has been accepted for publication in a future issue of this journal, but has not been fully edited. Content may change prior to final publication. Citation information: DOI 10.1109/TCOMM.2019.2936354, IEEE Transactions on Communications

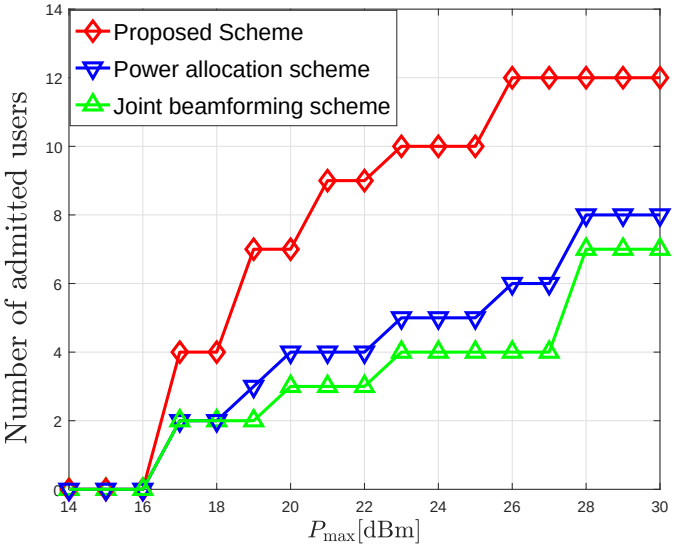

Fig. 7. Number of admitted users versus the maximum power budget per UAV with different interference management scheme.

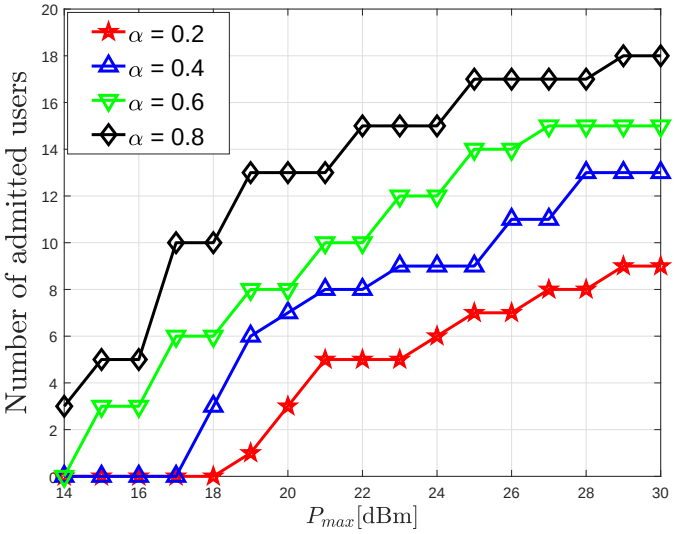

Fig. 8. Number of admitted users versus the maximum power budget per UAV with different values of α.

VII. Conclusion

In this paper, we have proposed and investigated a novel network architecture enabled by multiple content-aware UAVs. By leveraging the new promising technology of UAVs and the existing and established techniques such as distributed antenna system and multicast beamforming, we utilize a system of multiple content-aware UAVs with limited storage capacity that can cooperate with each other to enhance the system performance. Further, by acknowledging the relationship among the UAVs' storage capacity, their locations, and their capability to cooperate, we formulate a novel optimization problem to maximize the user admission, taking into consideration some practical constraints. Since our formulated problem is a mixed-integer non-convex optimization problem whose search of the optimal solution cannot be guaranteed a polynomial time, we proposed a framework based on difference-of-convex programming to approximate it into a series of mixed-integer second-order cone programs and iteratively solve them until convergence. Our simulation results reveal the superiority of our scheme compared to previous work from the literature and offer notable insights into the system operation as a function of a wide range of design parameters.

Appendix A
Proof of Theorem 1

First, we can rewrite $R_{jk}(\mathbf{w},\theta)$ as

$$R_{jk}(\mathbf{w},\theta) = \log\Big(\sum_{k\in\mathscr{K}} \left|(\mathbf{h}_{jk}(\theta_{jk}))^{\dagger}\mathbf{w}_k\right|^2 + \sigma_0^2\Big) - \tag{32}$$

$$\log\Big(\sum_{\ell\neq k} \left|(\mathbf{h}_{jk}(\theta_{jk}))^{\dagger}\mathbf{w}_\ell\right|^2 + \sigma_0^2\Big) \tag{33}$$

The gradient vector of $R_{jk}(\mathbf{w},\theta)$ is defined as $\nabla R_{jk}(\mathbf{w},\theta) = \left[\nabla_{\mathbf{w}} R_{jk}(\mathbf{w},\theta); \nabla_{\theta} R_{jk}(\mathbf{w},\theta)\right]$, with

$$\nabla_{\mathbf{w}} R_{jk}(\mathbf{w},\theta) = \underbrace{\frac{2\mathbf{w}^{\dagger}\mathbf{H}_{jk}(\theta)}{\mathbf{w}^{\dagger}\mathbf{H}_{jk}(\theta)\mathbf{w}+\sigma_0^2}}_{\bar{h}_1(\mathbf{w},\theta)\bar{h}_2(\mathbf{w},\theta)} - \underbrace{\frac{2\mathbf{w}^{\dagger}\tilde{\mathbf{H}}_{jk}(\theta)}{\mathbf{w}^{\dagger}\tilde{\mathbf{H}}_{jk}\mathbf{w}+\sigma_0^2}}_{\underline{\mathrm{h}}_1(\mathbf{w},\theta)\underline{\mathrm{h}}_2(\mathbf{w},\theta)} \tag{34}$$

$$\nabla_{\theta} R_{jk}(\mathbf{w},\theta) = \underbrace{\frac{2\theta^{\dagger}\Omega_{jk}(\mathbf{w})}{\mathbf{w}^{\dagger}\Omega_{jk}(\mathbf{w})\mathbf{w}+\sigma_0^2}}_{\bar{h}_3(\mathbf{w},\theta)\bar{h}_2(\mathbf{w},\theta)} - \underbrace{\frac{2\theta^{\dagger}\tilde{\Omega}_{jk}(\mathbf{w})}{\mathbf{w}^{\dagger}\tilde{\Omega}_{jk}(\mathbf{w})\mathbf{w}+\sigma_0^2}}_{\underline{\mathrm{h}}_3(\mathbf{w},\theta)\underline{\mathrm{h}}_2(\mathbf{w},\theta)} \tag{35}$$

In (34), we define $\hat{\mathbf{H}}_{jk}(\theta) = \mathbf{h}_{jk}(\theta_{jk})(\mathbf{h}_{jk}(\theta_{jk}))^{\dagger}$ to support the notational purpose of $\mathbf{H}_{jk}(\theta) = \mathrm{Bdiag}\underbrace{\left(\hat{\mathbf{H}}_{jk}(\theta),\ldots,\hat{\mathbf{H}}_{jk}(\theta)\right)}_{U\text{elements}}$ and $\tilde{\mathbf{H}}_{jk}(\theta) = \mathrm{Bdiag}\underbrace{\left(\hat{\mathbf{H}}_{jk}(\theta),\ldots,0,..,\hat{\mathbf{H}}_{jk}(\theta)\right)}_{U\text{elements}}$, where 0 appears at the k-th element. In (35), we define $\omega_{jk}(\mathbf{w}_k) = \mathbf{w}_k \circ \mathbf{h}_k$, $\omega'_{jk} = \omega_{jk}(\mathbf{w})(\omega_{jk}(\mathbf{w}))^{\dagger}$ to support the notational purpose of $\Omega_{jk}(\mathbf{w}) = \sum_{k\in\mathscr{K}} \omega'_{jk}$ and $\tilde{\Omega}_{jk}(\mathbf{w}) = \sum_{l\in\mathscr{K}\setminus k} \omega'_{jl}$. Then, we attempt to find Lipschitz constants for $\nabla_{\mathbf{w}} R_{jk}(\mathbf{w},\theta)$ and $\nabla_{\theta} R_{jk}(\mathbf{w},\theta)$. First, we have

$$\begin{aligned}
&\left\|\bar{h}_1(\mathbf{w},\theta) - \bar{h}_1(\mathbf{w}^{(0)},\theta^{(0)})\right\| \\
&= \|2\mathbf{w}^{\dagger}\mathbf{H}_{jk}(\theta) - 2\mathbf{w}^{(0)\dagger}\mathbf{H}_{jk}\left(\theta^{(0)}\right) + \\
&2\mathbf{w}^{\dagger}\mathbf{H}_{jk}\left(\theta^{(0)}\right) - 2\mathbf{w}^{\dagger}\mathbf{H}_{jk}\left(\theta^{(0)}\right)\| \\
&\leq \left\|2\mathbf{w}^{\dagger}(\mathbf{H}_{jk}(\theta) - \mathbf{H}_{jk}\left(\theta^{(0)}\right))\right\| \\
&+ \left\|2(\mathbf{w}-\mathbf{w}^{(0)})^{\dagger}\mathbf{H}_{jk}\left(\theta^{(0)}\right)\right\| \\
&\leq 2\|\mathbf{w}\| \left\|\mathrm{Bdiag}\left(\left(\mathbf{h}_{jk}(\theta_{jk}) - \mathbf{h}_{jk}(\theta_{jk})\right)\left(\mathbf{h}_{jk}(\theta_{jk})\right)^{\dagger}\right)\right\|_F \\
&+ 2\|\mathbf{w}\| \left\|\mathrm{Bdiag}\left(\mathbf{h}_{jk}(\theta_{jk}^{(0)})\left(\mathbf{h}_{jk}(\theta_{jk}) - \mathbf{h}_{jk}(\theta_{jk}^{(0)})\right)^{\dagger}\right)\right\|_F \\
&+ 2\left\|\mathbf{w}-\mathbf{w}^{(0)}\right\| \left\|\mathbf{H}_{jk}(1/H)\right\|_F \\
&\leq 2\|\mathbf{w}\| 2U \left\|\mathbf{h}_{jk}(1/H)\right\| \left\|\tilde{\mathbf{h}}_{jk}\right\|_{\infty} \left\|\theta_{jk} - \theta_{jk}^{(0)}\right\| \\
&+ 2\left\|\mathbf{w}-\mathbf{w}^{(0)}\right\| \left\|\mathbf{H}_{jk}(1/H)\right\|_F \leq
\end{aligned} \tag{36}$$

$$A_1\left(\left\|\theta-\theta^{(0)}\right\| + \left\|\mathbf{w}-\mathbf{w}^{(0)}\right\|\right) \tag{37}$$

This article has been accepted for publication in a future issue of this journal, but has not been fully edited. Content may change prior to final publication. Citation information: DOI 10.1109/TCOMM.2019.2936354, IEEE Transactions on Communications

with

$$A_1 = \max\left\{4U^2 P_{\max}\left\|\mathbf{h}_{jk}(1/H)\right\|\left\|\tilde{\mathbf{h}}_{jk}\right\|_\infty, 2\left\|\mathbf{H}_j(1/H)\right\|_F\right\}$$

In other words, the Lipschitz constant of $\bar{h}_1(\mathbf{v})$ is A_1. Similarly, we can derive

$$\left\|\bar{h}_2(\mathbf{w},\theta) - \bar{h}_2(\mathbf{w}^{(0)},\theta^{(0)})\right\| \leq B_1\left(\left\|\theta-\theta^{(0)}\right\| + \left\|\mathbf{w}-\mathbf{w}^{(0)}\right\|\right) \quad (38)$$

where $B_1 = 1/N_0^2(A_1/2 + UP_{\max}\left\|\mathbf{H}_j(1/H)\right\|_F$. Using (36) and (38), we can find the Lipschitz constant $\mathscr{A}_1$ of $\bar{h}_1(\mathbf{w},\theta)\bar{h}_2(\mathbf{w},\theta)$ as

$$\left\|\bar{h}_1(\mathbf{w},\theta)\bar{h}_2(\mathbf{w},\theta) - \bar{h}_1(\mathbf{w}^{(0)},\theta^{(0)})\bar{h}_2(\mathbf{w}^{(0)},\theta^{(0)})\right\| \leq \underbrace{\left(2UP_{\max}\left\|\mathbf{H}_{jk}(1/H)\right\|_F B_1 + 1/N_0 A_1\right)}_{\mathscr{A}_1} \times \left(\left\|\theta-\theta^{(0)}\right\| + \left\|\left(\mathbf{w}-\mathbf{w}^{(0)}\right)\right\|\right) \quad (39)$$

Similarly, we can derive the Lipschitz constant of $\bar{h}_3(\mathbf{w},\theta)$ as

$$\left\|\bar{h}_3(\mathbf{w},\theta) - \bar{h}_3(\mathbf{w}^{(0)},\theta^{(0)})\right\| \leq C_1\left(\|\theta-\theta^{(0)}\| + \left\|\left(\mathbf{w}-\mathbf{w}^{(0)}\right)\right\|\right) \quad (40)$$

where $C_1 = \max\left\{4U^2/H\left\|\tilde{\mathbf{h}}_{jk}\right\|_\infty^2 P_{\max}, 2UP_{\max}\left\|\tilde{\mathbf{h}}_{jk}\right\|_\infty\right\}$. Then, we can also find the Lipschitz constant $\mathscr{B}_1$ of $\bar{h}_3(\mathbf{w},\theta)\bar{h}_3(\mathbf{w},\theta)$ as

$$\left\|\bar{h}_3(\mathbf{w},\theta)\bar{h}_2(\mathbf{w},\theta) - \bar{h}_3(\mathbf{w}^{(0)},\theta^{(0)})\bar{h}_2(\mathbf{w}^{(0)},\theta^{(0)})\right\| \leq \underbrace{\left(2U/H2UP^{\max}\left\|\tilde{\mathbf{h}}_{jk}\right\|_\infty B_1 + 1/N_0 C_1\right)}_{\mathscr{B}_1} \times \left(\left\|\theta-\theta^{(0)}\right\| + \left\|\left(\mathbf{w}-\mathbf{w}^{(0)}\right)\right\|\right) \quad (41)$$

By following the same steps, we can also conclude that the Lipschitz constants for the terms $\underline{\mathrm{h}}_k(\mathbf{w},\theta), k = 1\ldots,3$ are A_1, B_1, C_1, respectively. Finally, we have

$$\left\|\nabla_{\mathbf{v}} R_{jk}(\mathbf{w},\theta) - \nabla_{\mathbf{v}} R_{jk}(\mathbf{w}^{(0)},\theta^{(0)})\right\| \leq \xi_0\left(\left\|\theta-\theta^{(0)}\right\| + \left\|\left(\mathbf{w}-\mathbf{w}^{(0)}\right)\right\|\right) \quad (42)$$

where $\xi_0 = 2\times\max\{\mathscr{A}_1, \mathscr{B}_1\}$. We now prove Theorem 1. According to (42), $R_{jk}(\mathbf{v},\theta)$ is ξ_0–smooth. Thus, we have

$$\|R_{jk}(\mathbf{w},\theta) - R_{jk}(\mathbf{w}^{(0)},\theta^{(0)}) - \nabla_{\mathbf{v}} R_{jk}(\mathbf{w}^{(0)},\theta^{(0)})^\intercal([\mathbf{w},\theta]-[\mathbf{w}^{(0)},\theta^{(0)}])\| \leq \frac{\xi_0}{2}(||\theta-\theta^{(0)}||^2 + ||\mathbf{w}-\mathbf{w}^{(0)}||^2) \quad (43)$$

which means

$$R_{jk}(\mathbf{w},\theta) \geq -\frac{\xi_0}{2}(\left\|\theta-\theta^{(0)}\right\|^2 + \left\|\left(\mathbf{w}-\mathbf{w}^{(0)}\right)\right\|^2) + R_{jk}(\mathbf{w}^{(0)},\theta^{(0)}) + \nabla R_{jk}(\mathbf{w}^{(0)},\theta^{(0)})^\intercal([\mathbf{w},\theta]-[\mathbf{w}^{(0)},\theta^{(0)}]) \quad (44)$$

Because of the strong convexity of $\xi_{jk}(\|\mathbf{w}\|^2 + \|\theta\|^2)$, we have

$$\xi_{jk}(\|\mathbf{w}\|^2 + \|\theta\|^2) \geq \xi_{jk}\left\|\mathbf{w}^{(0)}\right\|^2 + \left\|\theta^{(0)}\right\|^2) + 2\xi_{jk}[\mathbf{w}^{(0)},\theta^{(0)}]^\intercal([\mathbf{w},\theta]-[\mathbf{w}^{(0)},\theta^{(0)}]) + \frac{\xi_{jk}}{2}(\left\|\theta-\theta^{(0)}\right\|^2 + \left\|\left(\mathbf{w}-\mathbf{w}^{(0)}\right)\right\|^2) \quad (45)$$

From the two inequalities (44)–(45), we obtain

$$f_{jk}(\mathbf{w},\theta) \geq \frac{\xi_{jk}-\xi_0}{2}(||\theta-\theta^{(0)}||^2 + ||\mathbf{w}-\mathbf{w}^{(0)}||^2) + f_{jk}(\mathbf{w}^{(0)},\theta^{(0)}) + \nabla f_{jk,t}(\mathbf{w},\theta)(\mathbf{w}^{(0)},\theta^{(0)})^\intercal([\mathbf{w},\theta]-[\mathbf{w}^{(0)},\theta^{(0)}])$$

which means that $R_{jk}(\mathbf{w},\theta)$ is strongly convex.

ACKNOWLEDGEMENT

The authors are grateful for the financial support provided by NSERC and by Concordia University.

REFERENCES

[1] P. Popovski, K. F. Trillingsgaard, O. Simeone, and G. Durisi, "5G wireless network slicing for eMBB, URLLC, and mMTC: A communication-theoretic view," *IEEE Access.*, vol. 6, Sept 2018.

[2] X. Wang, L. Kong, F. Kong, F. Qiu, M. Xia, S. Arnon, and G. Chen, "Millimeter wave communication: A comprehensive survey," *IEEE Commun. Surveys Tuts.*, vol. 20, no. 3, pp. 1616–1653, June 2018.

[3] E. G. Larsson, O. Edfors, F. Tufvesson, and T. L. Marzetta, "Massive MIMO for next generation wireless systems," *IEEE Commun. Mag.*, vol. 52, no. 2, February 2014.

[4] D. López-Pérez, M. Ding, H. Claussen, and A. H. Jafari, "Towards 1 Gbps/UE in cellular systems: Understanding ultra-dense small cell deployments," *IEEE Commun. Surveys Tuts.*, vol. 17, no. 4, pp. 2078–2101, June 2015.

[5] L. Gupta, R. Jain, and G. Vaszkun, "Survey of important issues in UAV communication networks," *IEEE Commun. Surveys Tuts.*, vol. 18, no. 2, pp. 1123–1152, Nov. 2015.

[6] A. A. Khuwaja, Y. Chen, N. Zhao, M. Alouini, and P. Dobbins, "A survey of channel modeling for UAV communications," *IEEE Commun. Surveys Tuts.*, vol. 20, no. 4, pp. 2804–2821, Jul 2018.

[7] M. F. Sohail, C. Y. Leow, and S. Won, "Non-orthogonal multiple access for unmanned aerial vehicle assisted communication," *IEEE Access.*, vol. 6, pp. 22 716–22 727, 2018.

[8] C. Zhan, Y. Zeng, and R. Zhang, "Energy-efficient data collection in UAV enabled wireless sensor network," *IEEE Wireless Commun. Lett.*, vol. 7, no. 3, pp. 328–331, June 2018.

[9] T. Bai, J. Wang, Y. Ren, and L. Hanzo, "Energy-efficient computation offloading for secure UAV-edge-computing systems," *IEEE Trans. Veh. Technol.*, vol. 68, no. 6, pp. 6074–6087, June 2019.

[10] S. Zeng, H. Zhang, K. Bian, and L. Song, "UAV relaying: Power allocation and trajectory optimization using decode-and-forward protocol," in *Proc. IEEE Int. Conf. Communications (ICC'18) Workshops*, 2018, pp. 1–6.

[11] X. Xu, Y. Zeng, Y. L. Guan, , and R. Zhang, "Overcoming endurance issue: UAV-enabled communications with proactive caching," *IEEE J. Sel. Areas Commun.*, vol. 36, no. 6, pp. 1231–1244, Jun 2018.

[12] U. Challita, W. Saad, and C. Bettstetter, "Interference management for cellular-connected UAVs: A deep reinforcement learning approach," *IEEE Trans. Wireless Commun.*, vol. 18, no. 4, pp. 2125–2140, April 2019.

[13] R. Irmer *et al.*, "Coordinated multipoint: Concepts, performance, and field trial results," *IEEE Commun. Mag.*, vol. 49, no. 2, pp. 102–111, Feb. 2011.

[14] S. Jeong, O. Simeone, and J. Kang, "Mobile edge computing via a UAV-mounted cloudlet: Optimization of bit allocation and path planning," *IEEE Trans. Veh. Technol.*, vol. 67, no. 3, pp. 2049 – 2063, May 2017.

[15] J. Liu, X. Wang, B. Bai, and H. Dai, "Age-optimal trajectory planning for UAV-assisted data collection," in *Proc. IEEE Conf. on Computer Commun. (INFOCOM 2018) Workshops*, Honolulu,HI, Dec. 2016.

[16] M. Alzenad, A. El-Keyi, and H. Yanikomeroglu, "3-D placement of an unmanned aerial vehicle base station for maximum coverage of users with different QoS requirements," *IEEE Commun. Lett.*, vol. 7, no. 1, pp. 38 – 41, Feb 2018.

[17] V. Sharma, R. Sabatini, and S. Ramasamy, "UAVs assisted delay optimization in heterogeneous wireless networks," *IEEE Commun. Lett.*, vol. 20, no. 12, pp. 2526 – 2529, Dec. 2016.

[18] Y. Chen *et al.*, "Optimum placement of UAV as relays," *IEEE Commun. Lett.*, vol. 22, no. 2, pp. 248–251, Feb 2018.

[19] M. M. Azari, F. Rosas, K.-C. Chen, and S. Pollin, "Joint sum-rate and power gain analysis of an aerial base station," in *Proc. IEEE Global Communications Conference (GLOBECOM 2016) Workshops*, Washington, DC, Dec. 2016.

[20] Y. Zeng and R. Zhang, "Energy-efficient UAV communication with trajectory optimization," *IEEE Trans. Wireless Commun.*, vol. 16, no. 6, pp. 3747–3760, Jun 2017.

[21] Y. Zeng, X. Xu, and R. Zhang, "Trajectory optimization for completion time minimization in UAV-enabled multicasting," *IEEE Trans. Wireless Commun.*, vol. 17, no. 4, pp. 2233 – 2246, Jan. 2018.

[22] N. Zhao *et al.*, "Caching UAV assisted secure transmission in hyper-dense networks based on interference alignment," *IEEE Trans. Commun.*, vol. 66, no. 5, pp. 2281 – 2294, May 2018.

[23] D. Jiang and Y. Cui, "Enhancing performance of random caching in large-scale wireless networks with multiple receive antennas," *IEEE Trans. Wireless Commun.*, vol. 18, no. 4, pp. 2051–2065, April 2019.

[24] N. Rupasinghe, Y. Yapıcı, . Güvenç, and Y. Kakishima, "Non-orthogonal multiple access for mmWave drone networks with limited feedback," *IEEE Trans. Commun.*, vol. 67, no. 1, pp. 762–777, Jan 2019.

[25] H. Pan, S. C. Liew, J. Liang, Y. Shao, and L. Lu, "Network-coded multiple access on unmanned aerial vehicle," *IEEE J. Sel. Areas Commun.*, vol. 36, no. 9, pp. 2071–2086, Sep. 2018.

[26] A. A. Nasir *et al.*, "UAV-enabled communication using NOMA," *IEEE Trans. Commun.*, 2019.

[27] Q. Wu, Y. Zeng, and R. Zhang, "Joint trajectory and communication design for multi-UAV enabled wireless networks," *IEEE Trans. Wireless Commun.*, vol. 17, no. 3, pp. 2109–2121, Mar. 2018.

[28] L. Wang and S. Zhou, "Energy-efficient UAV deployment with flexible functional split selection," in *Proc. IEEE 19th International Workshop on Signal Process. Advances in Wireless Commun. (SPAWC)*, Anaheim, CA, June 2018.

[29] L. Liu, S. Zhang, and R. Zhang, "CoMP in the sky: UAV placement and movement optimization for multi-user communications," *IEEE Trans. Commun.*, Mar. 2019.

[30] M. Amade *et al.*, "Information-centric networking for the internet of things: challenges and opportunities," *IEEE Netw.*, vol. 30, no. 2, pp. 92–100, Mar 2016.

[31] P. Dinh, T. M. Nguyen, C. Assi, and W. Ajib, "Joint beamforming and location optimization for cooperative content-aware UAVs," in *Proc. IEEE Wireless Comm. Net. Conf. (WCNC'19)*, Marrakech, Morocco, Apr. 2019, pp. 1–7.

[32] H. He, S. Zhang, Y. Zeng, and R. Zhang, "Joint altitude and beamwidth optimization for UAV-enabled multiuser communications," *IEEE Wireless Commun. Lett.*, vol. 22, no. 2, pp. 344–347, Feb. 2018.

[33] Q. Yuan, Y. Hu, C. Wang, and Y. Li, "Joint 3D beamforming and trajectory design for UAV-enabled mobile relaying system," *IEEE Access.*, vol. 7, pp. 26 488–26 496, 2019.

[34] T. M. Nguyen, A. Yadav, W. Ajib, and C. Assi, "Resource allocation in two-tier wireless backhaul heterogeneous networks," *IEEE Trans. Wireless Commun.*, vol. 15, no. 10, pp. 6690–6704, Oct 2016.

[35] B. R. Marks and G. P. Wright, "Technical note–A general inner approximation algorithm for nonconvex mathematical programs," *Operations Research*, vol. 26, pp. 681–683, Aug 1978.

[36] Q.-D. Vu, K.-G. Nguyen, and M. Juntti, "Max-min fairness for multicast multigroup multicell transmission under backhaul constraints," in *GLOBECOM 2016*, Washington, DC, Dec. 2016, pp. 1–6.

[37] MOSEK ApS, *The MOSEK optimization toolbox for MATLAB manual. Version 9.0.*, 2019. [Online]. Available: http://docs.mosek.com/9.0/toolbox/index.html

[38] A. Ghosh, R. Ratasuk, B. Mondal, N. Mangalvedhe, and T. Thomas, "LTE-advanced: next-generation wireless broadband technology [invited paper]," *IEEE Wireless Commun.*, vol. 17, no. 3, pp. 10–22, June 2010.

[39] H. Riiser, "Adaptive bitrate video streaming over HTTP in mobile wireless networks," Ph.D. dissertation, University of Oslo, Norway, 2013.

[40] M. Tao, E. Chen, H. Zhou, and W. Yu, "Content-centric sparse multicast beamforming for cache-enabled cloud RAN," *IEEE Trans. Wireless Commun.*, vol. 15, no. 9, pp. 6118–6131, Sep 2016.